BCSJ Award Article

Investigations of Electronic Structures and Photocatalytic Activities under Visible Light Irradiation of Lead Molybdate Replaced with Chromium(VI)

Yoshiki Shimodaira,[1] Hideki Kato,[1] Hisayoshi Kobayashi,[2] and Akihiko Kudo*[1,3]

[1]Department of Applied Chemistry, Faculty of Science, Science University of Tokyo, 1-3 Kagurazaka, Shinjuku-ku, Tokyo 162-8601

[2]Department of Chemistry and Materials Technology, Kyoto Institute of Technology, Matsugasaki, Sakyo-ku, Kyoto 606-8585

[3]Core Research for Evolutional Science and Technology, Japan Science and Technology Agency (CREST, JST), 4-1-8 Honcho, Kawaguchi 332-0012

Received October 17, 2006; E-mail: a-kudo@rs.kagu.tus.ac.jp

Chromium-replaced $PbMoO_4$, $PbMo_{1-x}Cr_xO_4$, prepared by an aqueous reflux method, showed a photocatalytic activity for O_2 evolution from an aqueous solution containing an electron accepter, such as Ag^+ or Fe^{3+} under visible light irradiation (vis) ($\lambda \geq 420$ nm). $PbMo_{0.98}Cr_{0.02}O_4$ (Energy gap: 2.26 eV) showed the highest activity for the O_2 evolution under vis and UV + vis light irradiation. The activity of $PbMo_{0.98}Cr_{0.02}O_4$ was one order of magnitude higher than that of $PbMoO_4$ under UV + vis light irradiation. The crystal structures of $PbMo_{1-x}Cr_xO_4$ were studied by the Rietveld analysis for powder X-ray diffraction. $PbMo_{1-x}Cr_xO_4$ had a scheelite-type structure when x was equal to or smaller than 0.2. The energy band structures of $PbMo_{1-x}Cr_xO_4$ were calculated based on density functional theory using the structural parameters refined by the Rietveld analysis. It was revealed that the top of the valence band of $PbMoO_4$ consisted of O2p and Pb6s orbitals and the accepter level was composed of a Cr3d orbital in the forbidden band below the conduction band consisting of a Mo4d orbital. It was concluded that the visible light response was due to the excitation from the Pb6s + O2p valence band to the Cr3d accepter level.

Photocatalytic water splitting into H_2 and O_2 is an important reaction from the viewpoint of the global energy and the environmental issues.[1,2] Recently, new photocatalysts consisting of metal ions with d^0 and d^{10} electron configurations have been developed for photocatalytic H_2 and O_2 evolution from water under UV irradiation, one after another.[1–10] Many of the new photocatalysts produce H_2 or O_2 from aqueous solutions containing sacrifice reagents under visible light irradiation. WO_3,[11–13] $RbPb_2Nb_3O_{10}$,[14] $BiVO_4$,[15–17] Bi_2WO_6,[18] and TiO_2 co-doped with Cr and Sb,[19] $AgNbO_3$,[20] Ag_3VO_4,[21] and Bi_2MoO_6[22] have been reported as active metal oxide photocatalysts for O_2 evolution from the aqueous solution containing the sacrificial reagents under visible light irradiation. On the other hand, $SrTiO_3$:Rh,[23] $SrTiO_3$:Cr,Ta,[24] $SrTiO_3$:Cr,Sb,[19] and $SnNb_2O_6$[25] are active metal oxides for H_2 evolution under visible light irradiation. Additionally, nitrides, oxynitrides, and oxysulfides, such as Ta_3N_5,[26] TaON,[27] and $Sm_2Ti_2S_2O_5$,[28] have been also reported as photocatalysts. Especially, the GaN:ZnO photocatalyst is active for water splitting into H_2 and O_2.[29,30] Some Z-scheme photocatalyst systems, which are active for water splitting under visible light irradiation, have been reported by using $SrTiO_3$:Cr,Ta, $SrTiO_3$:Rh, and TaON as H_2 evolution photocatalysts, and WO_3, $BiVO_4$, Bi_2MoO_6 as O_2 evolution photocatalysts.[31–33] Therefore, new visible light driven photocatalysts are important even if they are active for half reactions of water splitting in the presence of sacrificial reagents.

We have developed visible light driven photocatalysts by doping or replacement of foreign elements into photocatalysts with wide band gaps.[2] The visible light responses are due to the transition from electron-donor levels consisting of the foreign elements to conduction bands of the host photocatalysts. In a similar manner, forming an electron-acceptor level is another strategy to make an energy gap narrower. In this photocatalyst, electrons are photoexcited from a valence band to the acceptor level under visible light irradiation.

It has been reported that $PbMoO_4$ (band gap: 3.31 eV) with scheelite-type structure, similar to $BiVO_4$, shows the photocatalytic activity for H_2 or O_2 evolution from an aqueous solution containing a sacrifice reagent under UV irradiation.[34] On the other hand, Bi6s orbitals in the $BiVO_4$ photocatalyst contribute to the formation of the valence band.[15–17] Therefore, the band

Published on the web May 14, 2007; doi:10.1246/bcsj.80.885

structure of scheelite-structured $PbMoO_4$ with Pb6s orbitals is interesting. The scheelite-type structure, expressed as $M_IM_{II}O_4$, consists of $M_{II}O_4$ tetrahedra and M_I atoms coordinated by eight oxygen atoms. This structure is flexible and accepts the pairing of the various charge ions. For example, $Na_{0.5}Bi_{0.5}MoO_4$ (B. G.: 3.10 eV) shows photocatalytic activity for O_2 evolution from the aqueous silver nitrate solution under UV irradiation.[35]

In the present paper, a new visible light driven photocatalyst material, based on the $PbMoO_4$ host photocatalyst, $PbMo_{1-x}Cr_xO_4$, was developed. The Mo^{6+} ions of M_{II} sites on the scheelite-type structure were replaced by Cr^{6+} ions of the same sixth group's element as Mo^{6+} in order to form the electron acceptor level and keep the charge balance. The $PbMo_{1-x}Cr_xO_4$ photocatalyst was characterized by X-ray diffraction, scanning electron microscope, and diffuse reflection spectroscopy. The energy structure is also discussed by the plane-wave-based density functional theory (DFT) calculations using the crystal structural data obtained by the least-square method and Rietveld analysis.

Calculation

The crystal structures of $PbMo_{1-x}Cr_xO_4$ powder were refined by the Rietveld analysis[36] of X-ray diffraction (RINT 2000, Rigaku) data using the computer program RIETAN-2000.[37] $PbMo_{0.9375}Cr_{0.0625}O_4$ ($\times 16$; $Pb_{16}Mo_{15}CrO_{64}$) and $PbMo_{0.8750}Cr_{0.1250}O_4$ ($\times 16$; $Pb_{16}Mo_{14}Cr_2O_{64}$), which were the suitable amounts of the replacement, were used as samples for band structural calculation.

Plane-wave-based DFT calculations were carried out on $CaMoO_4$, $PbMoO_4$, and $PbMo_{1-x}Cr_xO_4$ by employing a CASTEP program.[38] The atomic coordinates of $PbMo_{0.9375}Cr_{0.0625}O_4$ and $PbMo_{0.8750}Cr_{0.1250}O_4$, refined by the Rietveld analysis, were used for the DFT calculations. The core electrons were replaced with ultrasoft core potentials,[39] and the valence electronic configurations for Ca, Pb, Mo, Cr, and O atoms were $3s^23p^64s^2$, $6s^25d^{10}6p^2$, $4s^24p^65s^14d^5$, $3s^23p^64s^13d^5$, and $2s^22p^4$, respectively. The calculations were carried out using the conventional unit cells of $[CaMoO_4]_2$, $[CaMoO_4]_{16}$, $[PbMoO_4]_2$, $[PbMoO_4]_{16}$, $[PbMo_{0.9375}Cr_{0.0625}O_4]_{16}$, and $[PbMo_{0.8750}Cr_{0.1250}O_4]_{16}$ for $CaMoO_4$, $PbMoO_4$, and $PbMo_{1-x}Cr_xO_4$ ($x = 1/16$ and $2/16$), respectively. The total numbers of the electrons were 96, 768, 104, 832, 832, and 832, respectively and the numbers of the occupied orbitals were 48, 384, 52, 416, 416, and 416, respectively. The kinetic energy cutoffs were taken to be 300 eV. A gradient-corrected (GGA) functional[40] and a PBE (Perdew, Burke, and Enzerhof) functional[41] were chosen as the types of a DFT exchange-correlation potential used in the calculation. The atomic coordinates of $CaMoO_4$ and $PbMoO_4$ were referenced from Gürmen et al.[42] and Lugli et al.,[43] respectively.

Experimental

$PbMo_{1-x}Cr_xO_4$ was synthesized by a reflux method. The starting materials used for the reflux reaction were $Pb(NO_3)_2$ (Wako Pure Chemicals; >99.5%), H_2MoO_4 (Kanto Chemical; purity >87.0% as MoO_3), and $K_2Cr_2O_7$ (Kanto Chemical; purity >99.9%). H_2MoO_4 was soaked in the mixed aqueous solution of $Pb(NO_3)_2$ and $K_2Cr_2O_7$ in a stoichiometric ratio. The solution was refluxed at atmospheric pressure using a mantle heater for 24 h. The products were washed with pure water, filtered, and dried at 320 K for 15 h in an oven. The phase purity of the obtained powders was confirmed by X-ray diffraction (Rigaku: MiniFlex). Surface areas were determined by BET measurement (Coulter; SA3100). Diffuse reflectance spectra were obtained using a UV–vis–NIR spectrometer (Jasco; Ubest U-570) and were converted from reflection to absorbance by the Kubelka–Munk method.

Photocatalytic O_2 evolution from an aqueous silver nitrate solution and H_2 evolution from an aqueous methanol solution were carried out in a gas-closed circulation system. The photocatalyst powder (0.5 g) was dispersed by a magnetic stirrer in an aqueous solution (0.05 mol L^{-1} $AgNO_3$ aq or 6.67 vol% MeOH aq, 320 mL) in a Pyrex reaction cell. The light source was a 300-W Xe lamp (ILC technology; CERMAX LX-300). Cut-off filters (HOYA) were employed for controlling wavelength of incident light. Pt cocatalysts were loaded from an aqueous H_2PtCl_6 (Tanaka Kikinzoku) solution by a photodeposition method. Amounts of evolved gases were determined using gas chromatography (Shimadzu, GC-8A, MS-5A, TCD, Ar carrier). Apparent quantum yields defined by Eq. 1 were measured using filters combined with band-pass (Kenko) and cut-off (HOYA) filters, and a photodiode (OPHIRA: PD300-UV of a head and NOVA of a powder monitor).

$$\text{A.Q.Y. (\%)} = \frac{\text{The number of reacted electrons}}{\text{The number of incident photons}} \times 100 = \frac{\text{The number of evolved } O_2 \text{ molecules} \times 4}{\text{The number of incident photons}} \times 100. \quad (1)$$

Results and Discussion

Structure Refinement. X-ray diffraction patterns of $PbMoO_4$, $PbMo_{1-x}Cr_xO_4$, and $PbCrO_4$ are shown in Fig. 1. The XRD patterns of $PbMo_{1-x}Cr_xO_4$ ($x \leq 0.2$), prepared by reflux, were in good agreement with the pattern of $PbMoO_4$ as shown in Fig. 1(1). The diffraction peaks shifted to a higher angle side of $PbMoO_4$ without broadening as the value of x increased as shown in Fig. 1(2). The successive shift in the XRD pattern indicated that the obtained crystals were not mixtures of $PbMoO_4$ (scheelite-type structure) and $PbCrO_4$ (non-scheelite-type structure) phases but pure scheelite-type phase of replaced $PbMo_{1-x}Cr_xO_4$ materials. The shift was reasonable because the ionic radius of a four coordinate Cr^{6+} ion (0.26 Å) is smaller than that of Mo^{6+} ion (0.41 Å) in tetrahedra.[44] Mixture phases of $PbMoO_4$ and $PbCrO_4$ were observed over 20% of the replaced amount of Cr^{6+}.

The lattice parameters of three $PbMo_{1-x}Cr_xO_4$ samples ($x = 0.0625$, 0.1, and 0.1250) were calculated by least-squares. The crystal system of $PbMoO_4$ was tetragonal with space group $I4_1/a$. Table 1 shows the calculated reciprocal-lattice and lattice parameters by the least-squares method. These parameters were reasonable, because the values of the residual sum of square Q[36] were very small. Figure 2 shows the trace of lattice parameters of $PbMo_{1-x}Cr_xO_4$. The a- and b-axes were shortened with an increase in the replaced amount of Cr^{6+} ion with a small ionic radius, while the c-axis slightly expanded. Therefore, the replacement of Cr^{6+} ion for Mo^{6+} ion is limited. Additionally, it was reasonable from the ionic radius

that the cell volume decreased with an increase in the replaced amount. The atomic coordinates of $PbMo_{0.9375}Cr_{0.0625}O_4$ ($\times 16$; $Pb_{16}Mo_{15}CrO_{64}$) and $PbMo_{0.8750}Cr_{0.1250}O_4$ ($\times 16$; $Pb_{16}Mo_{14}Cr_2O_{64}$) were refined further by Rietveld analysis using these parameters obtained by the least-squares method. These refinements of $PbMo_{0.9375}Cr_{0.0625}O_4$ and $PbMo_{0.8750}Cr_{0.1250}O_4$ gave agreement factors of $Rp = 9.27$ and 9.76%, $Rwp = 11.42$ and 13.74%, and $S = Rwp/Re = 1.27$ and 1.62, respectively. These atomic coordinates were used for DFT calculations. Table 2 shows the relationship between the M–O distance and the O–M–O angles of MO_4 (M = Cr and Mo) tetrahedra in $PbMo_{1-x}Cr_xO_4$ using DFT calculation models. The M–O distance became shorter gradually as the amount of Cr replacement increased. Moreover, because the six O–M–O angles of general regular tetrahedra are 109.5 degrees, the distortion in the MO_4 tetrahedra became larger as the value of x increased. This result also indicates that the scheelite structure is difficult with a large amount of Cr replacement.

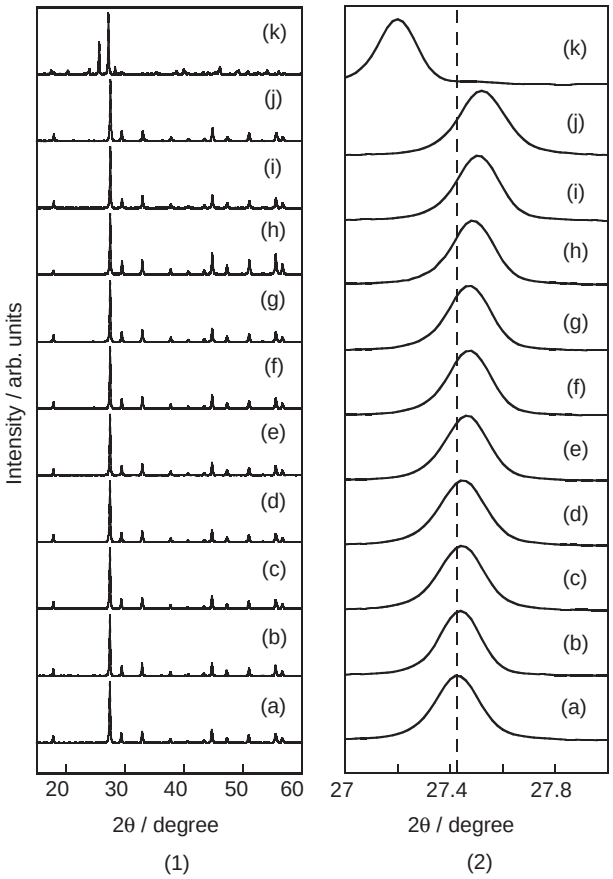

Fig. 1. X-ray diffraction patterns of $PbMo_{1-x}Cr_xO_4$ photocatalysts prepared by a reflux method; the values of x are: (a) 0, (b) 0.002, (c) 0.01, (d) 0.015, (e) 0.02, (f) 0.03, (g) 0.04, (h) 0.06, (i) 0.1, (j) 0.2, and (k) 1.

Electronic Structure Calculations. The band structures of $CaMoO_4$, $PbMoO_4$, $PbMo_{0.9375}Cr_{0.0625}O_4$, and $PbMo_{0.875}Cr_{0.125}O_4$ were studied by using plane-wave-based DFT in order to clarify which orbitals contribute to formation of the valence band, conduction band, and impurity level. Figures 3–6 show the band structure, the density of states (DOS), and the density contour maps for $CaMoO_4$, $PbMoO_4$, $PbMo_{0.9375}Cr_{0.0625}O_4$, and $PbMo_{0.875}Cr_{0.125}O_4$. The DFT calculations for $CaMoO_4$ and $PbMoO_4$ were carried out using two types of unit

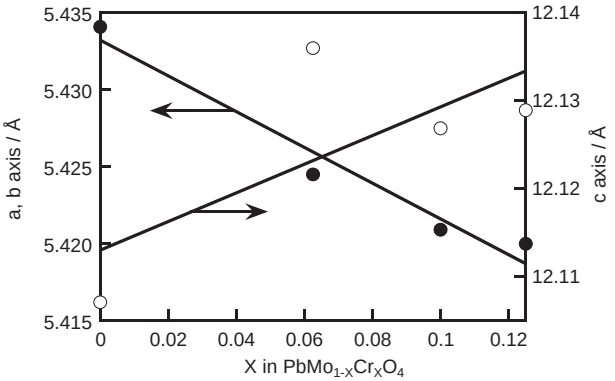

Fig. 2. Plots for calculated lattice parameters of $PbMo_{1-x}Cr_xO_4$: lattice parameters of $PbMoO_4$ are based on ICSD #89034.

Table 1. Reciprocal-Lattice and Lattice Parameters of $PbMo_{1-x}Cr_xO_4$

	$PbMoO_4$[a)]	$PbMo_{0.9375}Cr_{0.0625}O_4$	$PbMo_{0.9}Cr_{0.1}O_4$	$PbMo_{0.875}Cr_{0.125}O_4$
a[b)], b[b)]/Å	—	0.184349	0.184471	0.184502
c[b)]/Å	—	0.082400	0.082462	0.082447
V[b)]/Å^3	—	0.002800	0.002806	0.002807
a, b/Å	5.4340	5.424510	5.420910	5.420010
c/Å	12.107	12.13589	12.12687	12.12893
V/Å^3	357.499	357.102	356.3630	356.3050
Residual (Q)	—	0.00000051	0.00000038	0.00000034

a) ICSD #89034. b) Reciprocal lattice parameters.

Table 2. Distance and Angle of MO_4 (M = Cr and Mo) Tetrahedra in $PbMo_{1-x}Cr_xO_4$

	$PbMoO_4$[a)]	$PbMo_{0.9375}Cr_{0.0625}O_4$	$PbMo_{0.875}Cr_{0.125}O_4$
M–O distance (average)/Å	1.77 × 4	1.71 × 4	1.65 × 4
O–M–O angle (average)/°	107.14 × 4	106.04 × 4	101.50 × 4
	112.78 × 2	116.58 × 2	126.97 × 2

a) ICSD #89034.

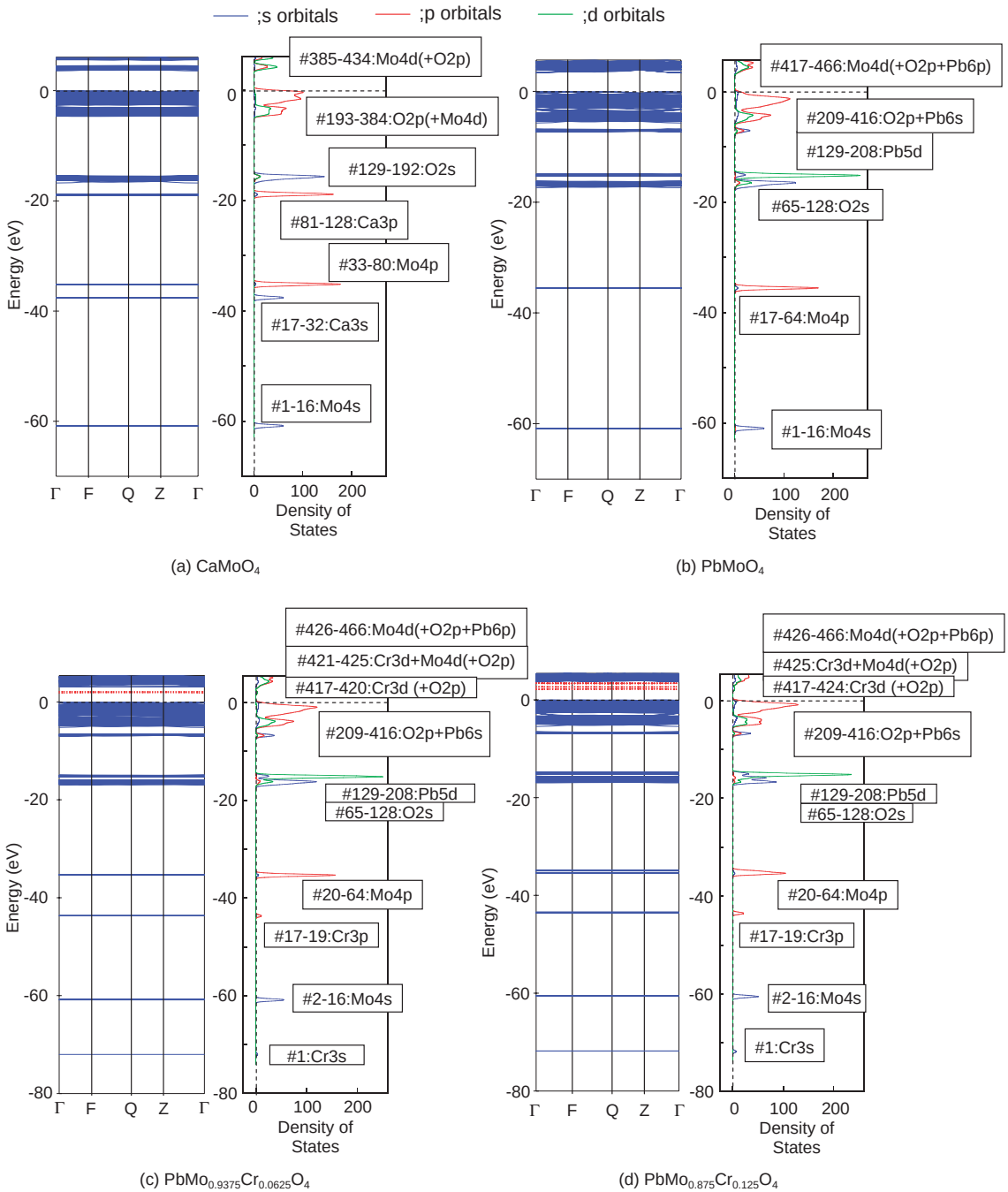

Fig. 3. Band structure and density of states: (a) $[CaMoO_4]_{16}$, (b) $[PbMoO_4]_{16}$, (c) $[PbMo_{0.9375}Cr_{0.0625}O_4]_{16}$, and (d) $[PbMo_{0.8750}Cr_{0.1250}O_4]_{16}$.

cells: conventional $[CaMoO_4]_2$ and $[PbMoO_4]_2$ cells and expanded $[CaMoO_4]_{16}$ and $[PbMoO_4]_{16}$ cells. Since there were scarcely any differences in the calculation results between these cells, only the cases of $[CaMoO_4]_{16}$ and $[PbMoO_4]_{16}$ are mentioned in this paper.

Band calculations for $CaMoO_4$ indicated that the valence band and the conduction band were derived from O2p and Mo4d orbitals, respectively, as seen in usual oxide materials consisting of d^0 metal cations. On the other hand, the top of the valence band including the HOMO of $PbMoO_4$ consisted of not only the O2p orbitals but also Pb6s orbitals partly unlike that of $CaMoO_4$ as shown in Figs. 3–5. Therefore, the Pb6s orbitals contributed to raising the valence band resulting in a narrower band gap of $PbMoO_4$ compared with that of $CaMoO_4$. On the other hand, the conduction band character of $PbMoO_4$ was similar to that of $CaMoO_4$. Even though there was a slight contribution from Ca4s and Ca3d orbitals on high energy sides of the conduction band, these orbitals were isolated, that is, not involved in the orbital of MoO_4 tetrahedra. A contribution from the Pb6p orbitals was also observed on high energy sides of the conduction band. These orbitals overlapped the region, in which there is a weak contribution from the MoO_4 tetrahedra. Accordingly, in contrast with the split conduction band of $CaMoO_4$, the conduction band of

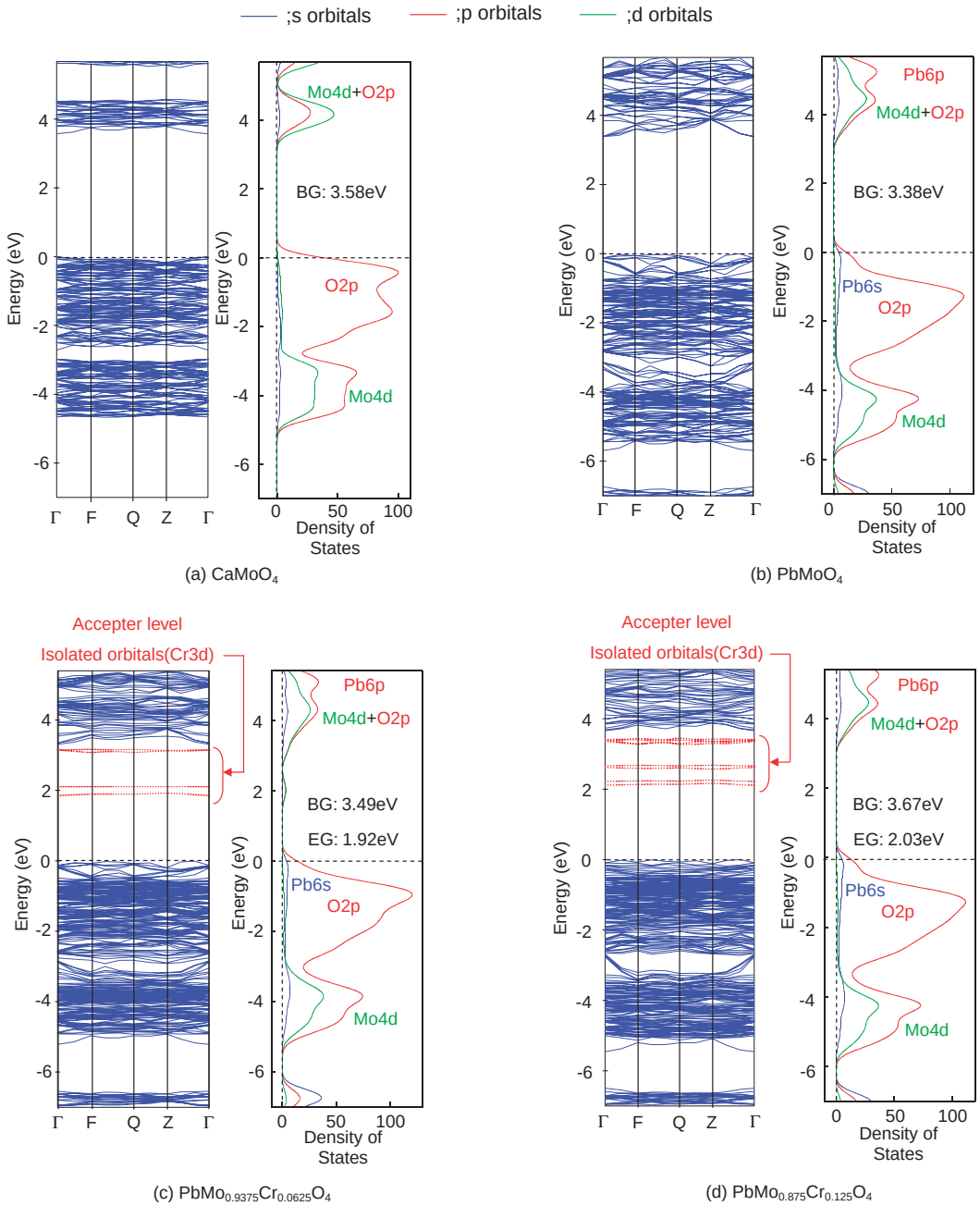

Fig. 4. Expanded band structure and density of states near band gap: (a) $[CaMoO_4]_{16}$, (b) $[PbMoO_4]_{16}$, (c) $[PbMo_{0.9375}Cr_{0.0625}O_4]_{16}$, and (d) $[PbMo_{0.8750}Cr_{0.1250}O_4]_{16}$.

$PbMoO_4$ is broad.

The valence bands of $PbMo_{0.9375}Cr_{0.0625}O_4$ and $PbMo_{0.875}Cr_{0.125}O_4$ consisted of hybrid orbitals of O2p and Pb6s orbitals as well as that of $PbMoO_4$ as shown in Figs. 3, 4, and 6. Although the characters of conduction bands for $PbMo_{0.9375}Cr_{0.0625}O_4$ (#421–425) and $PbMo_{0.875}Cr_{0.125}O_4$ (#425) were similar to that of $PbMoO_4$, Cr3d orbitals were also observed at the bottom of conduction band. Moreover, new electron accepter levels, derived from Cr3d orbitals, were also observed below the conduction bands of $PbMo_{0.9375}Cr_{0.0625}O_4$ and $PbMo_{0.875}Cr_{0.125}O_4$ as shown in Figs. 3, 4, and 6.

In regard to the conduction band of these Cr-replaced materials, in $PbMo_{0.9375}Cr_{0.0625}O_4$, the hybrid orbitals of Mo4d and Cr3d orbitals contributed to the lower region (#421–425), whereas only Mo4d orbitals contributed to the higher region of the conduction band (#426–#466). On the other hand, in the conduction band of $PbMo_{0.875}Cr_{0.125}O_4$, the degree of hybridization of the Mo4d and Cr3d orbitals was small, because the hybrid orbital was observed at only #425. The Cr3d of $PbMo_{0.875}Cr_{0.125}O_4$ orbitals almost contributed to the accepter level as a mini-band in band gap region (#417–424). This result indicated that the certain increase in the amount of the Cr^{6+} replacement made the hybridization of Cr3d and Mo4d orbitals weaken in the orbital group forming the conduction band. The gap between the conduction band consisting of Mo4d orbitals and the valence band consisting of O2p + Pb6s

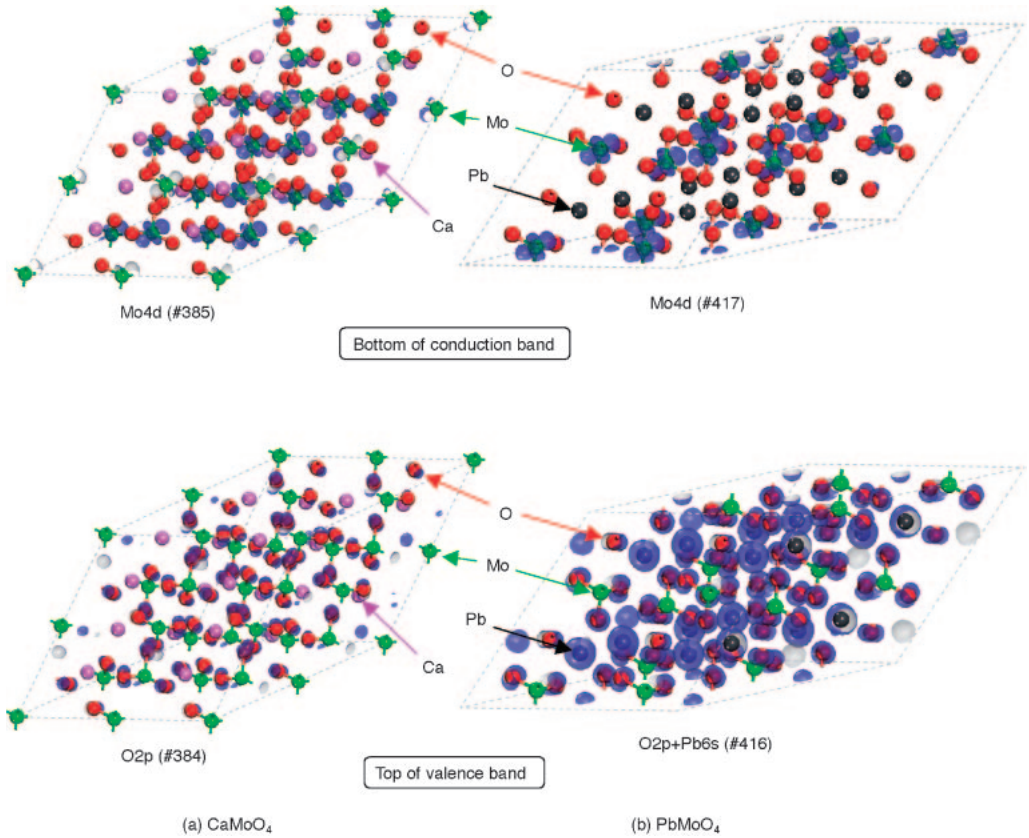

Fig. 5. Density contour maps for the top of valence band and the bottom of conduction band: (a) $[CaMoO_4]_{16}$, (b) $[PbMoO_4]_{16}$.

orbitals became wide with the increase in the distortion of the crystal structure by the increase in the amount of Cr^{6+} replacement as shown in Fig. 2 and Table 2. DFT calculations indicated that the band gaps of $PbMo_{0.9375}Cr_{0.0625}O_4$ and $PbMo_{0.8750}Cr_{0.1250}O_4$ were 3.49 and 3.67 eV, respectively, as shown in Fig. 4. The shift in the conduction band to a high energy level by the distortion caused the Cr3d level dissociation from the conduction band. Therefore, the difference in the contribution of the Cr3d level to the conduction band formation between $PbMo_{0.9375}Cr_{0.0625}O_4$ and $PbMo_{0.8750}Cr_{0.1250}O_4$ seemed to be observed. Thus, it was concluded that the increase in the amount of Cr^{6+} replacement might increase the localization of Cr3d and the transmutation from an isolated accepter level to a mini-band of Cr3d orbitals.

Figure 7 shows diffuse reflectance spectra of $CaMoO_4$, $PbMoO_4$, and $PbMo_{1-x}Cr_xO_4$. The band gap of $PbMoO_4$ (3.31 eV) was narrower than that of $CaMoO_4$ (3.80 eV) by replacement of Pb^{2+} ion for Ca^{2+} ion. The spectra of $PbMo_{1-x}Cr_xO_4$ showed new intensive absorption bands in the visible light region in addition to the band gap absorption band of $PbMoO_4$ in the ultraviolet region. The energy gaps of $PbMo_{1-x}Cr_xO_4$ became narrow as the value of x increased and were estimated to be 2.43–2.16 eV ($x = 0.002$–0.2) from the onsets of the absorption edge.

From the results of DRS measurements and DFT calculations, the band structure of the scheelite-type molybdates was developed as shown in Fig. 8. The valence and conduction bands of $CaMoO_4$ consisted of O2p and Mo4d orbitals, respectively. In contrast, the valence band of $PbMoO_4$ consisted of the hybrid orbitals of O2p and Pb6s, although the conduction band consisted of Mo4d orbital as well as that of $CaMoO_4$. The negative shift in the valence band by Pb6s orbitals was about 0.5 eV. In $PbMo_{1-x}Cr_xO_4$, there was an isolated accepter level derived from Cr3d orbitals at 1.1–1.2 eV below the conduction band bottom. These valence and conduction bands were similar to these of $PbMoO_4$, although the Cr3d orbital contributed slightly to the conduction bands for $PbMo_{1-x}Cr_xO_4$. Therefore, it was concluded that, based on $CaMoO_4$, the visible light response was achieved by simultaneously controls of the valence band and the accepter level in the present study. It is suggested that the replacement of elements to keep the charge balance and to make electron-donor and -accepter levels in a forbidden band is one of the effective ways to develop active photocatalysts with visible light response.

Photocatalytic Activities. The photocatalytic activities of $PbMo_{1-x}Cr_xO_4$ are summarized in Table 3. $PbMoO_4$ showed the photocatalytic activities for H_2 and O_2 evolution from aqueous methanol and silver nitrate solutions, respectively, under UV irradiation, respectively. However, Cr-replaced materials showed no H_2 evolution activity under not only vis but also UV irradiation. It indicated that the accepter level consisting of Cr3d was lower than the reduction potential of H_2O to form H_2. Moreover, excited electrons should easily fall into the accepter level from conduction band under UV irradiation. $PbMo_{0.98}Cr_{0.02}O_4$ showed the highest photocatalytic activity for O_2 evolution under UV + vis irradiation. The excited electrons were transferred to accepter level and reduced the Ag^+ ions. $PbMo_{0.98}Cr_{0.02}O_4$ showed higher photocatalytic activity

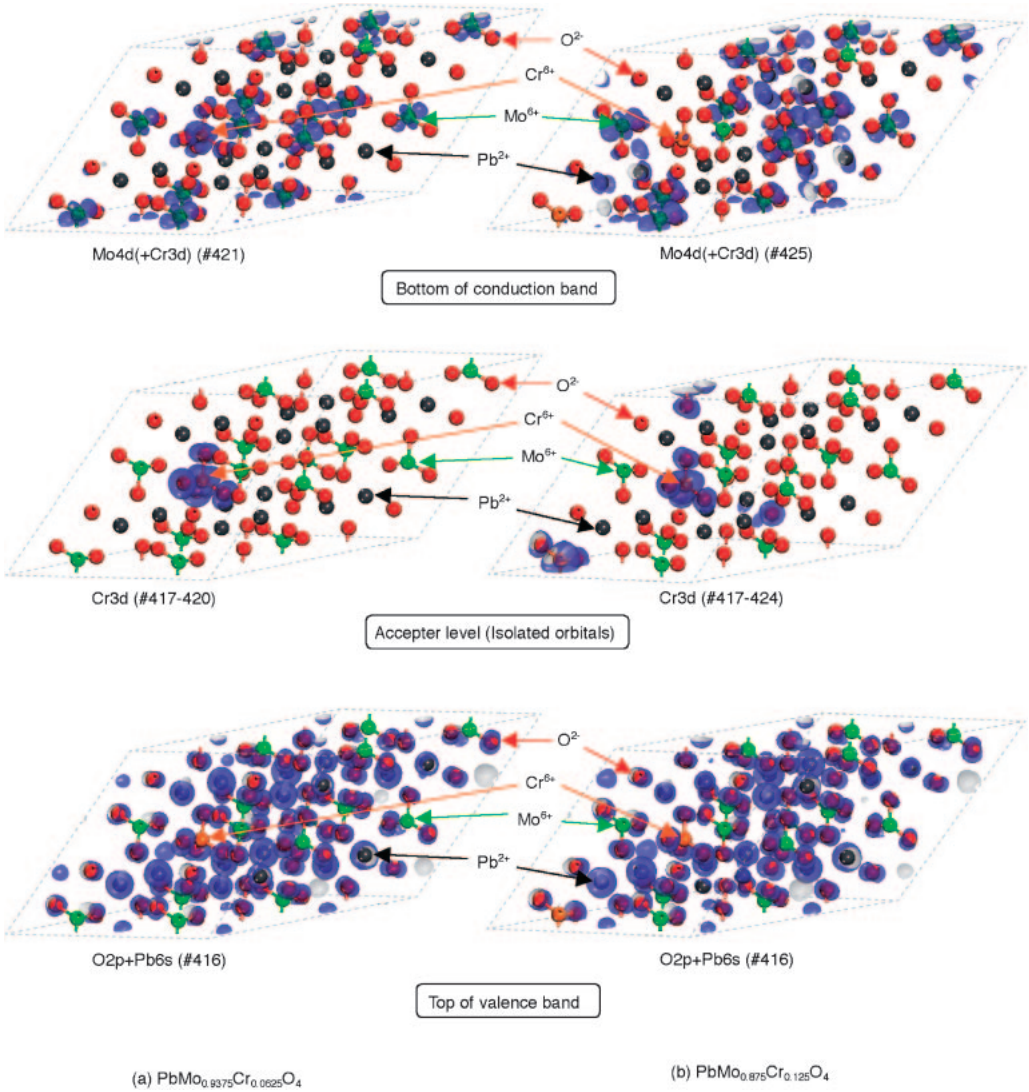

Fig. 6. Density contour maps for the top of valence band, the accepter level, and the bottom of conduction band: (a) $[PbMo_{0.9375}Cr_{0.0625}O_4]_{16}$, and (b) $[PbMo_{0.8750}Cr_{0.1250}O_4]_{16}$.

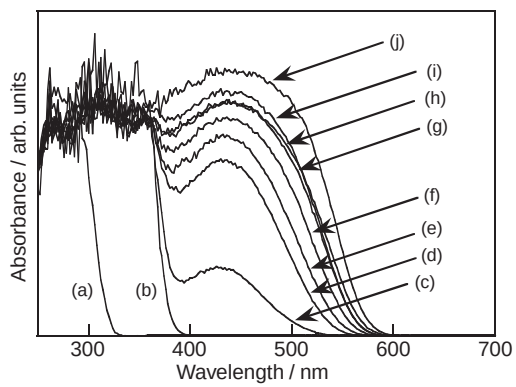

Fig. 7. Diffuse reflectance spectra of (a) $CaMoO_4$, and (b–j) $PbMo_{1-x}Cr_xO_4$ photocatalysts; the values of x are: (b) 0, (c) 0.002, (d) 0.01, (e) 0.02, (f) 0.03, (g) 0.04, (h) 0.06, (i) 0.1, and (j) 0.2.

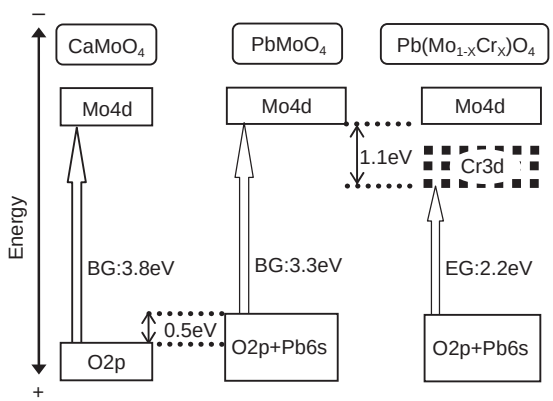

Fig. 8. Band structures of $CaMoO_4$ and $PbMo_{1-x}Cr_xO_4$.

than $PbMoO_4$ under full-arc irradiation, because the number of available photon for the Cr-replaced $PbMo_{0.98}Cr_{0.02}O_4$ was more than that for the non-replaced $PbMoO_4$.

Figure 9 shows the relationship between the amount of replacement and the photocatalytic activity for O_2 evolution under vis irradiation. Replaced Cr element increases the visible light response, whereas it negatively acts as a recombination

Table 3. Photocatalytic Activities of $PbMo_{1-x}Cr_xO_4$

Photocatalyst	E.G. /eV	Incident light /nm	Activity/μmol h^{-1}	
			H_2[a)]	O_2[b)]
$Pb(Mo_{0.80}Cr_{0.20})O_4$	2.16	$\lambda > 420$	0	9.8
$Pb(Mo_{0.90}Cr_{0.10})O_4$	2.18	$\lambda > 420$	0	12.8
$Pb(Mo_{0.94}Cr_{0.06})O_4$	2.20	$\lambda > 420$	0	19.8
$Pb(Mo_{0.96}Cr_{0.04})O_4$	2.21	$\lambda > 420$	0	33.2
$Pb(Mo_{0.97}Cr_{0.03})O_4$	2.23	$\lambda > 420$	0	62.0
		$\lambda > 300$	0	91.6
$Pb(Mo_{0.98}Cr_{0.02})O_4$	2.26	$\lambda > 420$	0	71.5
		$\lambda > 300$	0	120.5
$Pb(Mo_{0.985}Cr_{0.015})O_4$	2.29	$\lambda > 420$	0	47.2
		$\lambda > 300$	0	72.0
$Pb(Mo_{0.99}Cr_{0.01})O_4$	2.32	$\lambda > 420$	0	20.6
$Pb(Mo_{0.998}Cr_{0.002})O_4$	2.43	$\lambda > 420$	0	2.6
		$\lambda > 300$	0	6.9
$PbMoO_4$	3.31	$\lambda > 300$	1.9	12.8

a) Sample: 0.5 g, Pt: 1.0 wt % 6.67 vol % MeOH aq: 320 mL, 300 W Xe-lamp (side). b) Sample: 0.5 g, 0.05 mol L^{-1} $AgNO_3$ aq: 320 mL, 300 W Xe-lamp (side).

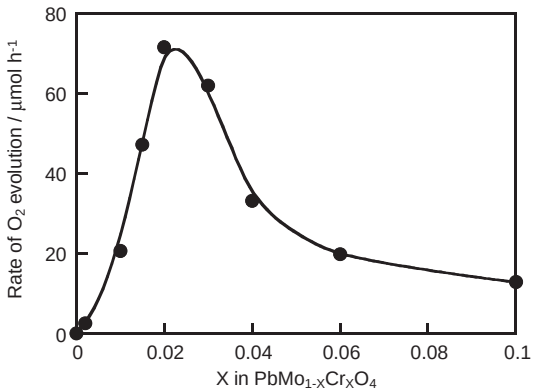

Fig. 9. Dependence of photocatalytic O_2 evolution from an aqueous $AgNO_3$ solution over $PbMo_{1-x}Cr_xO_4$ under visible-light irradiation ($\lambda > 420$ nm) upon the amount of Cr-replacement. Sample: 0.5 g, $AgNO_3$ aq (0.05 M 320 mL), 300 W Xe-lamp.

center between photogenerated electron and holes. When x was smaller than 0.02, the activity decreased. This is due to the isolation of a Cr3d accepter level and a decrease in the number of available photons. On the other hand, the activity for O_2 evolution decreased as the value of x became larger than 0.02. In these compositions, the function as a recombination center became predominant. In general, the activities of the doped photocatalysts with visible-light response are lower than those of non-doped materials even by band gap excitation.[19,23,45] It is mainly due to the charge balance kept by the Cr^{6+} replacement.

The photocatalytic reaction for O_2 evolution from an aqueous silver nitrate solution proceeds through paths (1)–(3) under visible light irradiation in $PbMo_{1-x}Cr_xO_4$ photocatalysts.

$$PbMo_{1-x}Cr_xO_4 \xrightarrow[\text{vis}]{} e^- \text{ (AL/Cr)} + h^+ \text{ (VB/Pb+O)}, \quad (1)$$

$$e^- \text{ (AL/Cr)} + Ag^+ \rightarrow Ag, \quad (2)$$

$$4h^+ \text{ (VB/Pb+O)} + 2H_2O \rightarrow O_2 + 4H^+. \quad (3)$$

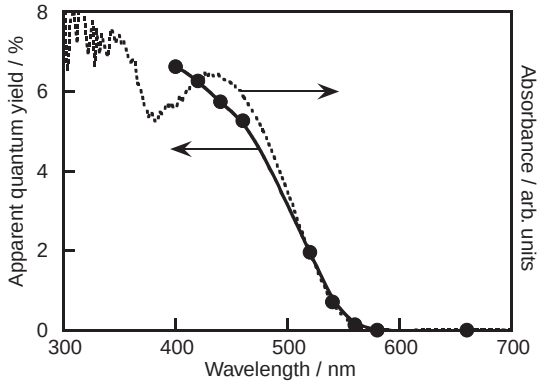

Fig. 10. Action spectrum for O_2 evolution from an aqueous $AgNO_3$ solution over $PbMo_{0.98}Cr_{0.02}O_4$ photocatalyst and diffuse reflectance spectrum: Sample: 0.5 g, $AgNO_3$ aq (0.05 M 320 mL), 300 W Xe-lamp.

One might think that the photogenerated electrons reduce Cr^{VI} and not Ag^+ to form ions with lower oxidation numbers, such as Cr^{III}.

$$3e^- + Cr^{VI} \rightarrow Cr^{III}. \quad (4)$$

If reaction (4) occurs, the corresponding amount of O_2 should form according to reaction (3). However, the reduction of Cr^{VI} was negligible because the reaction using pure water, instead of an aqueous silver nitrate solution, gave no O_2. This result indicated that Cr^{VI} in the lattice of the $PbMo_{1-x}Cr_xO_4$ photocatalyst was stable toward reduction. On the other hand, photocatalytic O_2 evolution was also observed from an aqueous iron(III) nitrate solution on a $PbMo_{0.98}Cr_{0.02}O_4$ photocatalyst, although the activity was lower than that from an aqueous silver nitrate solution.

$$e^- \text{ (AL/Cr)} + Fe^{3+} \rightarrow Fe^{2+}. \quad (5)$$

Thirty-four micromoles of O_2 were obtained after a reaction of 10 h indicating that 136 μmol of e^- and h^+ reacted. There was 27.3 μmol of Cr in 0.5 g of a $PbMo_{0.98}Cr_{0.02}O_4$ photocatalyst. The amount of reacted electrons was more than that required for the reduction of Cr^{VI} to, for example, Cr^{III}. This result also indicated that the reduction of Cr^{VI} in the photocatalyst was negligible.

Figure 10 shows an action spectrum for the O_2 evolution from an aqueous Ag^+ solution over a $PbMo_{0.98}Cr_{0.02}O_4$ photocatalyst. The onset of the action spectrum agreed well to that of the diffuse reflectance spectrum. It was shown that the visible-light response of the photocatalyst was due to the energy gap transition between the valence band and the accepter level. The apparent quantum yield of $PbMo_{0.98}Cr_{0.02}O_4$ photocatalyst was 6% at 420 nm; it was comparatively high for the photocatalyst with visible-light response due to the formation of a impurity level.

Conclusion

Chromium-replaced $PbMoO_4$ with scheelite-type structure showed intense absorption bands in the visible light region. Thus, $PbMo_{1-x}Cr_xO_4$ is a new visible light-driven photocatalyst for O_2 evolution from an aqueous solution. The photocatalytic activity depended on the amount of Cr^{VI}-replacement.

$PbMo_{0.98}Cr_{0.02}O_4$ showed the highest activity. DFT calculations and DRS measurement indicated that the position of the electron-accepter level consisting of Cr3d orbitals was around 1.1–1.2 eV below the conduction band bottom. The negative shift in the valence band by Pb6s orbitals was observed by comparison with $CaMoO_4$. The present study indicates that the formation of the electron-accepter level by a foreign element with keeping a charge balance is one strategy to develop new visible light driven photocatalysts.

This work has been supported by Core Research for Evolutional Science and Technology (CREST) of Japan Science and Technology Agency (JST) and Grant-in-Aid (No. 14050090) for the priority Area Research (No. 417) from the Ministry of Education, Culture, Sports, Science and Technology.

References

1 K. Domen, J. N. Kondo, M. Hara, T. Takata, *Bull. Chem. Soc. Jpn.* **2000**, *73*, 1307.
2 A. Kudo, H. Kato, I. Tsuji, *Chem. Lett.* **2004**, *33*, 1534.
3 J. Sato, H. Kobayashi, K. Ikarashi, N. Saito, H. Nishiyama, Y. Inoue, *J. Phys. Chem. B* **2004**, *108*, 4369.
4 T. Ishihara, H. Nishiguchi, K. Fukamachi, Y. Takita, *J. Phys. Chem. B* **1999**, *103*, 1.
5 K. Ikarashi, J. Sato, N. Saito, H. Nishiyama, Y. Inoue, *J. Phys. Chem. B* **2002**, *106*, 9048.
6 J. Sato, N. Saito, H. Nishiyama, Y. Inoue, *J. Phys. Chem. B* **2003**, *107*, 7965.
7 J. Sato, N. Saito, Y. Yamada, K. Maeda, T. Takata, J. N. Kondo, M. Hara, H. Kobayashi, K. Domen, Y. Inoue, *J. Am. Chem. Soc.* **2005**, *127*, 4150.
8 M. Machida, K. Mitsuyama, K. Ikeue, S. Matsushima, S. Arai, *J. Phys. Chem. B* **2005**, *109*, 7801.
9 K. Shimizu, S. Itoh, T. Hatamachi, T. Kodama, M. Sato, K. Toda, *Chem. Mater.* **2005**, *17*, 5161.
10 H. Otsuka, K. Kim, A. Kouzu, I. Takimoto, H. Fujimori, Y. Sakata, H. Imamura, T. Matsumoto, K. Toda, *Chem. Lett.* **2005**, *34*, 822.
11 A. A. Krasnovsky, G. P. Brin, *Dokl. Akad. Nauk* **1962**, *147*, 656.
12 J. R. Darwent, A. Mills, *J. Chem. Soc., Faraday Trans. 2* **1982**, *78*, 359.
13 W. Erbs, J. Desilvestro, E. Borgarello, M. Greatzel, *J. Phys. Chem.* **1984**, *88*, 4001.
14 J. Yoshimura, Y. Ebina, J. Kondo, K. Domen, A. Tanaka, *J. Phys. Chem.* **1993**, *97*, 1970.
15 A. Kudo, K. Ueda, H. Kato, I. Mikami, *Catal. Lett.* **1998**, *53*, 229.
16 A. Kudo, K. Omori, H. Kato, *J. Am. Chem. Soc.* **1999**, *121*, 11459.
17 S. Tokunaga, H. Kato, A. Kudo, *Chem. Mater.* **2001**, *13*, 4624.
18 A. Kudo, S. Hijii, *Chem. Lett.* **1999**, 1103.
19 H. Kato, A. Kudo, *J. Phys. Chem. B* **2002**, *106*, 5029.
20 H. Kato, H. Kobayashi, A. Kudo, *J. Phys. Chem. B* **2002**, *106*, 12441.
21 R. Konta, H. Kato, H. Kobayashi, A. Kudo, *Phys. Chem. Chem. Phys.* **2003**, *5*, 3061.
22 Y. Shimodaira, H. Kato, H. Kobayashi, A. Kudo, *J. Phys. Chem. B* **2006**, *110*, 17790.
23 R. Konta, T. Ishii, H. Kato, A. Kudo, *J. Phys. Chem. B* **2004**, *108*, 8992.
24 T. Ishii, H. Kato, A. Kudo, *J. Photochem. Photobiol., A* **2004**, *163*, 181.
25 Y. Hosogi, K. Tanabe, H. Kato, H. Kobayashi, A. Kudo, *Chem. Lett.* **2004**, *33*, 28.
26 M. Hara, G. Hitoki, T. Takata, J. N. Kondo, H. Kobayashi, K. Domen, *Catal. Today* **2003**, *78*, 555.
27 M. Hara, G. Hitoki, T. Takata, J. N. Kondo, H. Kobayashi, K. Domen, *Stud. Surf. Sci. Catal.* **2003**, *145*, 169.
28 A. Ishikawa, T. Takata, J. N. Kondo, M. Hara, H. Kobayashi, K. Domen, *J. Am. Chem. Soc.* **2002**, *124*, 13547.
29 K. Maeda, T. Takata, M. Hara, N. Saito, Y. Inoue, H. Kobayashi, K. Domen, *J. Am. Chem. Soc.* **2005**, *127*, 8286.
30 K. Maeda, K. Teramura, D. Lu, T. Takata, N. Saito, Y. Inoue, K. Domen, *Nature* **2006**, *440*, 295.
31 K. Sayama, A. Nomura, Z. Zou, R. Abe, Y. Abe, H. Arakawa, *Chem. Commun.* **2003**, 2908.
32 H. Kato, M. Hori, R. Konta, Y. Shimodaira, A. Kudo, *Chem. Lett.* **2004**, *33*, 1348.
33 R. Abe, T. Takata, H. Sugihara, K. Domen, *Chem. Commun.* **2005**, 3829.
34 A. Kudo, A. Steinberg, A. J. Bard, A. Campion, M. A. Fox, T. E. Mallouk, S. E. Webber, J. M. White, *Catal. Lett.* **1990**, *5*, 61.
35 H. Kato, N. Matsudo, A. Kudo, *Chem. Lett.* **2004**, *33*, 1216.
36 H. Miura, *J. Ceram. Soc. Jpn.* **1997**, *105*, 584.
37 F. Izumi, T. Ikeda, *Mater. Sci. Forum* **2000**, *321*, 198.
38 M. C. Payne, M. P. Teter, D. C. Allan, T. A. Arias, *Rev. Mod. Phys.* **1992**, *64*, 1045.
39 D. Vanderbilt, *Phys. Rev. B* **1990**, *41*, 7892.
40 J. A. White, D. M. Bird, *Phys. Rev. B* **1994**, *50*, 4954.
41 J. P. Perdew, K. Burke, M. Ernzerhof, *Phys. Rev. Lett.* **1996**, *77*, 3865.
42 E. Gürmen, E. Daniels, J. S. King, *J. Chem. Phys.* **1971**, *55*, 1093.
43 C. Lugli, L. Medici, D. Saccardo, *Neues Jahrb. Mineral., Monatsh.* **1999**, *6*, 281.
44 R. D. Shannon, *Acta Crystallogr., Sect. A* **1976**, *32*, 751.
45 I. Tsuji, A. Kudo, *J. Photochem. Photobiol., A* **2003**, *156*, 249.